The physics behind the hypothesis of alternation

G. Petrillo[1], **A. Rosso**[2] **& E. Lippiello**[1]

[1]Department of Mathematics and Physics, University of Campania "L. Vanvitelli", Viale Lincoln 5, 81100 Caserta, Italy
[2]LPTMS, CNRS, Univ. Paris-Sud, Université Paris-Saclay, 91405 Orsay, France

Key Points:

- We investigate the hypothesis of alternation in a physical model of a seismic fault presenting realistic features of aftershock occurrence
- We find that aftershocks do not occur in large-slip areas which become relocked and the next mainshock occurs in different fault regions
- We find that the time until the next big shock is inversely proportional to the percentage of aftershocks inside the mainshock slip contour

Corresponding author: Eugenio Lippiello, `eugenio.lippiello@unicampania.it`

Abstract

The hypothesis of alternation leads to the idea of immunity after local disaster which, notwithstanding it sounds reasonable, it has been frequently rejected by objective testing. More generally the estimate of the occurrence probability of the next big shock on the basis of the time delay from the last earthquake still represents a big challenge. The problem is that this issue cannot be addressed only on the basis of historical catalogs which contain to few well documented big shocks and decades of future observations appear necessary. On the other hand, recent results have shown that important insights can be obtained from the spatial organization of aftershocks and its relationship to the mainshock slip profile. Here we address this issue by monitoring the stress evolution together with the occurrence of big shocks and their aftershocks in a physical model where the seismic fault is described as an elastic layer embedded in a ductile medium. The model reproduces all relevant statistical features of earthquake occurrence and allows us to perform accurate testing of the hypothesis of alternation and its consequences, particularly on the side of aftershock spatial patterns. We demonstrate that the hypothesis of characteristic earthquakes is not valid but that is possible to achieve insights on the time until the next big shock on the basis of the percentage of aftershocks occurring inside the high slip contour of the mainshock.

1 Introduction

The hypothesis of alternation dates back to Gilbert (1909) and states that "When a large amount of stored energy has been discharged in the production of a great earthquake and its after-shocks, it would seem theoretically that the next great seismic event in the same seismic district was more likely to occur at some other place, and that successive great events would be distributed with a sort of alternation through the districts..." In the same manuscript, however, Gilbert concluded "..its corollary of local immunity after local disaster is more alluring than safe".

After 115 years from the fundamental warning raised by Gilbert, the range of validity of his hypothesis of "alternation" is not yet fixed. In particular, after the development of the elastic rebound theory, the hypothesis of alternation has been gradually replaced by a stronger hypothesis which is usually termed seismic gap or seismic cycle model. This model assumes that consecutive earthquakes substantially re-rupture the same fault segment, nucleating characteristic earthquakes which are roughly equal in size and roughly periodic in time. As a consequence the terms gap model and characteristic earthquake model are often used as synonyms and several predictions have been accordingly formulated for different geographic regions, as for instance in (McCann et al., 1979) and (Nishenko, 1991). This model is still often adopted in earthquake prediction even if many studies (Kagan & Jackson, 1991; Rong et al., 2003) have shown that the gap hypothesis can be rejected with a high confidence level and, as stated by Mulargia et al. (2017), "no recent work makes a strong data-based case in support of these predictions". In particular, the spatio-temporal organization of events considered by Rong et al. (2003) appears more consistent with the scenario where large earthquakes follow a Poisson process in time where large earthquake occurrence is fully unpredictable. Nevertheless, the failure of the gap model, intended as characteristic model, does not imply the failure of the alternation hypothesis as originally formulated by Gilbert. Indeed, the situation becomes more intriguing if one relaxes the assumption of a characteristic size and location of subsequent earthquakes and takes into account the possibility that subsequent ruptures are allowed to have only partial overlaps. This has recently done in a study (Roth et al., 2017) conducted along the South American subduction zone for the last 500 years, which shows that recurrence times of magnitude $m \geq 7$ earthquakes present some tendencies towards short-time clustering. This result, which is apparently in opposition to the hypothesis of alternation, can be still consistent with it if one takes into account that in the data analysis of Roth et al. (2017) only the overlap between epicentral coordinates is taken into account and that most of the $m \gtrsim 7$ earthquakes rupture only a part of the seismogenic width. Consistently with the hypothesis of alternation, indeed, the partial rupture can cause the stress increase along the unbroken part of the fault width which, in turn, can raise the probability of subsequent earthquakes with similar epicentral coordinates in the near future. This scenario is avoided if one restricts the study to magnitude $m \geq 8$ earthquakes, which are sufficiently large to rupture the full seismogenic zone. Interestingly, in this case Roth et al. (2017) find a weak quasi-periodic temporal organization of events, consistent with the hypothesis of alternation. The problem in this case is that the statistical sample is so small, only 20 recurrences, that a definite conclusion cannot be drawn. To this extent one should need data with a much more accurate hypocentral localization or a much larger statistical sample, not available from historical seismicity. In particular, because of the long time interval between big shocks, many decades of observations would be necessary to have an appropriate sample to statistically address this issue.

Here we try to give an immediate answer to the fundamental question about the validity of the hypothesis of alternation by recasting to the information provided by realistic physical models for seismic faults. In particular we present results for a physical model which is able to capture the complex magnitude-spatio-temporal pattern of seismicity, including the occurrence of aftershocks. This last feature can provide very useful insights on the hypothesis of alternation as recently shown by Wetzler et al. (2018). Indeed, the stress loading mechanism behind the hypothesis of alternation predicts that aftershocks must be located outside the region involved during the mainshock slip or, at most, in regions with low levels of the mainshock slip. This peculiar aftershock pattern has been recently enlightened in real data by Wetzler et al. (2018) after considering 101 large subduction zone plate boundary mainshocks with well determined coseismic slip distributions. This accurate study has revealed a deficit of aftershocks inside the mainshock slip area consistently with the hypothesis of large slip areas re-locking. The observation that larger aftershocks typically occur farther away than smaller ones (van der Elst & Shaw, 2015) represents another feature of aftershock occurrence supporting the hypothesis of alternation. More generally, framing the organization of aftershocks in space, time and magnitude within the hypothesis of alternation could lead to very useful predictions for the occurrence of the next large earthquake. A striking example is represented by the very interesting prediction, proposed by Wetzler et al. (2018), that the temporal distance to the subsequent larger earthquake is smaller the larger is the number of aftershocks inside the high slip contour of the mainshock. Indeed, according to the hypothesis of alternation, an intense aftershock activity inside the mainshock high-slip zone could suggest that the mainshock has released only a small portion of the accumulated shear stress and therefore one could expect a shortest waiting time up to the next mainshock. This prediction can be easily put in a testable form but, taking still into account that the occurrence of large earthquakes with overlapping slip regions is a rare event, its experimental validation will need decades of observations.

Results of Wetzler et al. (2018) therefore reveals the importance of physical models with realistic spatio-temporal patterns of aftershocks in order to test ideas and at the same time to improve existing predictions. Here we demonstrate that it is possible to recover all the main predictions of the hypothesis of alternation within a physical model which quantitatively reproduces the relevant scaling laws of aftershock occurrence. The model, indeed, also reproduces the GR law which is a well established empirical law indicating that earthquake magnitudes follow an exponential distribution covering a broad magnitude range, in opposition to the seismic cycle model which predicts that only a characteristic value of the magnitude should be observed. The model we consider is a generalization of the Burridge-Knopoff (BK) (Burrige & Knopoff, 1967) model where the seismic fault is described as an elastic interface composed of springs and blocks subject to a velocity-weakening friction law. The original BK model, however, does not produce a "genuine" aftershock activity which is instead observed if the BK interface is embedded in a more ductile region (Petrillo et al., 2020). This is modeled as a second extended interface subject to velocity-strengthening rheology and, because of the coupling between the two interfaces, the stress drop of large earthquakes induces an afterslip dynamics (Perfettini & Avouac, 2004, 2007) in the velocity strengthening layer. This in turn triggers the occurrence of aftershocks in the velocity weakening layer and this mechanism leads to an aftershock number which decays in time as a power law, as predicted by the Omori law (Omori, 1894).

A complete description of the physical model is given in (Petrillo et al., 2020) where also the main results about the spatio-temporal organization of simulated earthquakes can be found. In the following section we describe the main features of the model with results presented in the subsequent section. The last section is devoted to discussions and conclusions.

2 The model

We consider a rectangular fault, of size $L_x = 15000a$ and $L_y = 200a$, modeled as an elastic layer composed of springs and blocks, where a is the rest length of the springs. The local stress on each block is the sum of two contributions f_i+g_i. The stress f_i originates from the elastic interaction with the other blocks of the fault layer whereas g_i is the stress induced by the interaction with the ductile region. The model exhibits three distinct phases: the slip phase corresponds to earthquake nucleation and slip propagation, the afterslip phase when aftershocks occur and the interseismic phase when the fault is locked. An earthquake is defined as a series of slips occurring during the slip phase and starting from the initial instability of the i-th block, whose position defines the epicentral coordinates of the earthquake. More precisely, the slip phase is entered as soon as the local stress f_i+g_i overcomes a local random frictional stress threshold τ_i^{th}. The block i is unstable and performs a slip with a stress drop Δf which leads to the following stress redistribution

$$\begin{aligned} f_i(t) &\rightarrow f_i(t) - 4\Delta f \\ f_j(t) &\rightarrow f_j(t) + \Delta f \\ g_i(t) &\rightarrow g_i(t) - 4\Theta\Delta f \\ g_j(t) &\rightarrow g_j(t) + (\Theta - \epsilon)\,\Delta f \end{aligned} \tag{1}$$

where j corresponds to the index of each of the four blocks on the fault which are nearest neighbor of the i-th block, whereas Θ and ϵ are two model parameters. In particular, $\Theta \in [0,1]$ quantifies the elastic interaction between the two layers and if $\Theta = 0$ the fault does not interact with the ductile layer whereas the maximum interaction is obtained when $\Theta = 1$. At the same time ϵ controls the amount of stress dissipated and when $\epsilon = 0$ all the stress drop of the i-th block is transferred to nearest neighbor block. Nevertheless, since blocks on the fault border have a number of nearest neighbor blocks smaller than four, a further dissipation mechanism is present also when $\epsilon = 0$.

After the slip of the block i the friction threshold is updated and a new value τ_i^{th} is extracted from a Gaussian distribution with mean $\overline{\tau}$ and standard deviation σ. The stress redistribution can cause the instability of one or more blocks j, leading to the propagation of the stress in further blocks via a cascading process. The slip phase, i.e. the earthquake, ends when $f_i + g_i < \tau_i^{th}$ in all sites.

We introduce the quantity $n_k(i)$ for the number of slips performed by the i-th block during the k-th earthquake and, since to each slip corresponds a stress drop Δf, the final local stress drop in the site i after the k-th earthquake is $\delta f_k(i) = n_k(i)\Delta f$. Therefore, the seismic moment M_k released during the k-th earthquake can be defined as $M_k \propto \sum_i \delta f_k(i)$, where the sum extends over all blocks. We finally define the moment magnitude $m_k = (2/3)\log_{10} M_k$, where we have set to zero the arbitrary additive constant.

Furthermore, for each earthquake k, we measure the maximum slip $n_k^{\max}$ as the maximum value of $n_k(i)$ over all blocks. We then define the χ-contour as the continuous line separating the region with $n_k(i) > \chi n_k^{\max}$ from the one with $n_k(i) < \chi n_k^{\max}$, where $\chi \in [0, 1]$. For $\chi = 0$ the χ-contour corresponds to the border of the slipped area. We also define the slipped area $A_k(\chi)$ as the total number of sites internal to the χ-contour, i.e. the total number of sites with $n_k(i) > \chi n_k^{max}$. Another measured quantity is the overlap $Q_{k,j}(\chi)$ between the earthquakes k and j, defined as the intersection between the slipped areas of the two earthquakes $A_k(\chi) \cap A_j(\chi)$. More precisely $Q_{k,j}(\chi)$ is defined as the sum over all blocks i such that $n_k(i) > \chi n_k^{max}$ and also $n_j(i) > \chi n_j^{max}$.

At the end of the slip phase, because of Eq.s (1), sites which have performed at least one slip during the earthquake present a negative value $g_i(t_0) < 0$. Nevertheless, because of the afterslip dynamics of the ductile layer the afterslip phase starts and $g_i(t)$ continues to evolve in time

$$g_i(t) = g_i(t_0)\Phi(t - t_0). \tag{2}$$

Here $\Phi(t)$ is a logarithmic decreasing function of time obtained from the stationary solution of the rate-and-state friction law ((Dieterich, 1972; Ruina, 1983; Chris, 1998; Lippiello, Petrillo, Landes, & Rosso, 2021)). The afterslip process Eq.(2) leads to a logarithmic increase of the local stress and eventually to the occurrence of an instability at time t_1 in the site j, such that $f_j + g_j(t_0)\Phi(t_1 - t_0) = \tau_j^{th}$. A new earthquake, i.e. an aftershock, then nucleates from the epicenter j and the slip phase is entered again. The process is iterated such as many aftershocks can be triggered and the afterslip phase ends when $g_i(t_{end}) = 0$ in all sites. At this point the inter-seismic phase starts with the stress $g_i(t)$ growing linearly in time $g_i(t) = (t - t_{end})\dot{g}$, where $\dot{g}$ is a very slow tectonic rate $\dot{g}$. The linear growth of $g_i(t)$ will lead to a new instability in a given site j where $f_j(t_{end}) + (t - t_{end})\dot{g} = \tau_j^{th}$ and, therefore, a new earthquake is triggered. The event triggered at the end of the inter-seismic phase is considered the first event of a new seismic sequence. The end of the seismic sequence corresponds to the end of the afterslip phase t_{end} and we define the mainshock as the largest earthquake in the sequence and its aftershocks or foreshocks are all subsequent or previous earthquakes, respectively, belonging to the same sequence.

The main assumptions of the model are that the slip and the subsequent stress redistribution Eq.s (1) occurs so fast that $\Phi(t)$ is constant during the whole slip phase. At the same time we assume that the stress rate $\dot{g}$ is such small that the effect of tectonic drive is negligible during the afterslip phase. Accordingly, we measure times in units of $t_d = \Delta f/\dot{g}$, which is the typical waiting time between two subsequent seismic sequences whereas the typical duration of an aftershock sequence is much smaller than t_d. We remark that our model, together with Θ and ϵ, presents only one extra parameter which is the standard deviation σ, which quantifies the level of friction heterogeneity. In the case $\Theta = 0$ and $\sigma = 0$ the model coincides with the Olami, Feder, Christensen (OFC) model (Olami et al., 1992) whereas for $\Theta = 0$ and $\sigma > 0$ the model corresponds to the elastic interface depinning model, sometimes defined OFC* model (de Arcangelis et al., 2016). Similar behaviors of the model with $\Theta > 0$ and $\sigma > 0$ are found in other models (Jagla, 2010; Jagla & Kolton, 2010; Jagla, 2011, 2013, 2014; F. m. c. P. Landes et al., 2015; Lippiello et al., 2015; F. P. Landes, 2016; F. P. Landes & Lippiello, 2016; Zhang & Shcherbakov, 2016) which generalize the OFC model by adding a relaxation mechanism responsible for aftershocks and implement heterogeneities in the friction thresholds τ_j^{th} .

We present results for a numerical catalog containing 10000 sequences, setting $\Theta = 0.5$ and $\sigma = 5$. We have verified that similar results are obtained for $\Theta \in [0.2, 0.7]$ and $\sigma > 2$. Furthermore we mostly focus only on mainshocks with $A_k(\chi = 0) > A^{th} = L_y^2$, i.e. earthquakes sufficiently large to expand over the whole seismogenic thickness L_y. Results do not depend on the specific value of A^{th} for sufficiently large A^{th}.

3 Results

In Fig.1a we present the temporal evolution of a numerical catalog by plotting the magnitude as function of the time. The figure clearly enlightens the presence of temporal clustering with aftershocks mostly concentrated soon after the occurrence of the largest earthquake of each sequence. Fig.1 also shows the efficiency of the model in reproducing the GR law. Indeed, we show that the magnitude distribution clearly follows an exponential law $P(m) \sim 10^{-bm}$ with $b \simeq 1$ up to values $m \lesssim 4$ (Fig.1b). The distribution becomes flatter at larger magnitudes, indicating that the number of $m \gtrsim 4$ earthquakes is larger than the one expected by extrapolating the small m behavior. As shown in (Petrillo et al., 2020) these deviations are caused by events with $A_k(\chi = 0) \gtrsim A^{th} = L_y^2$ which span over the whole vertical direction, whereas for $L_y \gg 1$ the GR law extends over a larger magnitude range. The behavior of Fig.1b therefore suggests the coexistence of the GR law with the occurrence of characteristic earthquakes which are sufficiently large to rupture the whole seismogenic depth. At the same time Fig.1c shows that the number of aftershocks exhibits an hyperbolic decay as function of the time since the mainshock, consistent with the instrumental Omori law.

In Fig.1d we plot the stress drop configuration after a typical large mainshock zooming in a region surrounding its epicenter. We observe that the stress drop is highly heterogeneous with the high-slip region mostly located around the epicenter whereas the stress drop slightly decreases approaching zero outside the $(\chi = 0)$-contour. In Fig.1d we also plot the epicentral positions of aftershocks showing that the majority of aftershocks are located close to the $(\chi = 0)$-contour. In particular the slipped area of the largest aftershocks mostly extend within regions where $n_k(i)/n_k^{\max} \lesssim 0.2$. In order to verify that the pattern observed in Fig.1d is a stable feature of all aftershock sequences, for each mainshock k, we sort its aftershocks in temporal order and indicate with $j(k) = 1, ..., n_k^{aft}$, the index associated to each aftershock. We have verified (Petrillo et al., 2020) that the total number of aftershocks n_k^{aft} exponentially depends on the magnitude of the mainshock, consistently with the productivity law (de Arcangelis et al., 2016). For each aftershock we measure the quantity $\Delta r_{j(k),k}(\chi)$ defined as the distance of the epicenter of the $j(k)$-th aftershock from the χ-contour of the k-th mainshock. We adopt the convention used in (Wetzler et al., 2018) to associate negative (positive) values to $\Delta r_{j(k),k}(\chi)$ if the aftershock epicenter is internal (external) to the χ contour. As clearly evident from Fig.1d the shape of the $(\chi = 0)$-contour is quite irregular, nevertheless we can define a typical size of the slipped area of the k-th mainshock, $R_k = \sqrt{A_k(\chi = 0)/\pi}$, which corresponds to assume a circular shape of the $(\chi = 0)$-contour. This allows us to obtain the spatial distribution of aftershocks averaging over mainshocks of different sizes by introducing the re-scaled variable $\Delta r_{j(k),k}(\chi)/R_k$. In the hypothesis of aftershocks homogeneously distributed within the slipped area, and under the assumption of a circular contour, the distribution of $\Delta r_{j(k),k}(\chi)/R_k$ is expected to linearly increase up to $\Delta r_{j(k),k}(\chi) = 0$. Results plotted in Fig.2a show instead a deficit of aftershocks with respect to the uniform distribution at small values of $\Delta r_{j(k),k}(\chi)/R_k < -0.5$ and conversely an excess when $\Delta r_{j(k),k}(\chi) \simeq 0$. This clearly indicates that the majority of aftershocks are spatially located close to the border of the slipped area whereas only few aftershocks occur well inside the slip contour. This feature becomes more evident the larger is the value of χ, indicating that the deficit of interior aftershocks becomes more pronounced when we consider high slip regions. This clearly supports the idea that high slip regions are more stable, in good agreement with the same analysis performed by (Wetzler et al., 2018) on real world mainshocks. We also observe that the deficit of interior aftershocks becomes more pronounced if one restricts the previous analysis to aftershocks with magnitude larger than a given magnitude threshold m_{th}. By increasing m_{th}, indeed, the number of interiors aftershock decreases (Fig.2b) whereas the peak close to $\Delta r_{j(k),k}(\chi) \simeq 0$ becomes more pronounced. This feature further supports the hypothesis of alternation indicating that the largest aftershocks preferentially occur in regions of low mainshock slip.

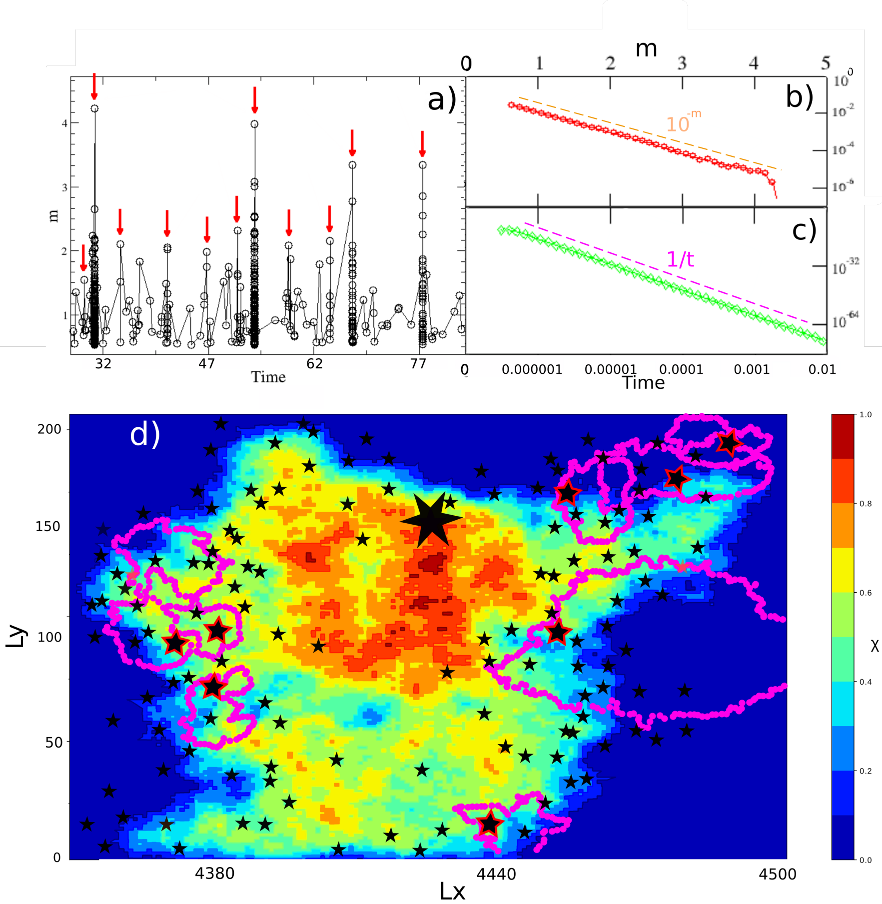

227 **Figure 1.** (a). A typical part interval of the numerical catalog containing 11 sequences. We plot the magnitude of each event m versus its occurrence time (in t_d units). Different arrows identify the temporal position of the mainshock in each sequence. According to our choice of model parameters, the duration of aftershock sequences is much smaller than t_d and aftershock occurrence appears roughly simultaneous to the mainshock occurrence. (b) The magnitude distribution $P(m)$. The orange dashed line is the GR law with $b = 1.0$. (c) The number of aftershocks as function of time since the mainshock. The magenta dashed line is the hyperbolic Omori decay $1/t$. (d) The stress drop configuration after a mainshock with epicentral coordinates $(4421a, 149a)$. Different colors correspond to different level of the stress drop χ as indicated in the color code. Pink circle dots represent the $\chi = 0$-contour of aftershocks with $m > 1.8$ whose epicenters are identified by black stars with red contour. Smaller black stars represent the epicenters of all $m > 1$ aftershocks. The big six-pointed star is the mainshock epicenter.

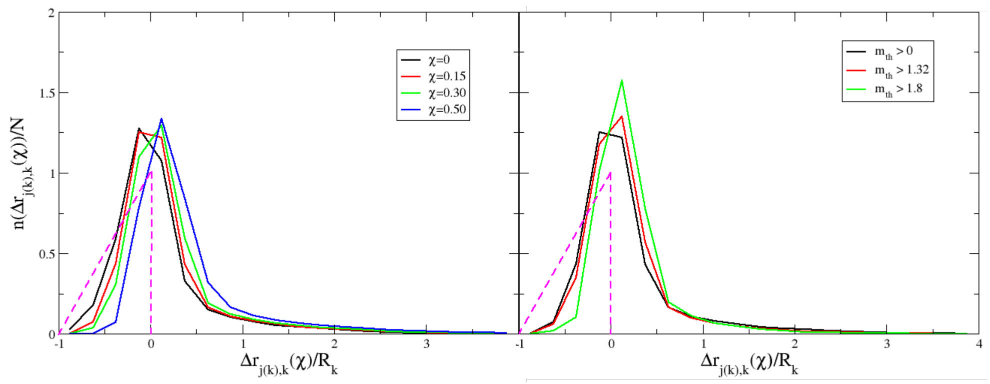

Figure 2. (a) The distribution of $\Delta r_{j(k),k}(\chi)/R_k$ for $m > 0$ aftershocks. Different colors correspond to different χ values. (b) The same as panel (a) keeping $\chi = 0$ fixed and considering aftershocks with magnitude larger than m_{th} and different m_{th} values.The dashed magenta line is the expected distribution in the case of aftershocks uniformly distributed in space within the slip area.

3.1 Correlation between pre-stress level and mainshock occurrence

We next define the pre-stress level, at the time $t = t_k$ immediately before the occurrence of the k-th mainshock, as

$$F_k^{\rm pre}(t) = \sum_{i \in C(R_k, x(k))} (f_i(t) + g_i(t)) \tag{3}$$

where $C(R_k, x(k))$ is a circle of radius $R_k = \sqrt{A_k(\chi = 0)}/\pi$ centered in $x(k)$, which is the centroid of the $(\chi = 0)$-contour. The above definition allows us to compare the actual pre-stress level on the slipped patch of the fault with the stress level $F_{k'}^{\rm pre}$ in other regions of the same fault and of the same size R_k. The quantity $F_{k'}^{\rm pre}$ is indeed defined as in Eq.(3) but replacing $C(R_k, x(k))$ with $C(R_k, x_{ran})$, i.e. a circle of the same radius R_k but with center in a random position x_{ran}. We apply periodic boundary conditions for the evaluation of $F_{k'}^{\rm pre}$. By exploring 1000 random positions x_{ran}, for each mainshock k, we evaluate the difference $\Delta F = F_k^{\rm pre}(t_k) - F_{k'}^{\rm pre}(t_k)$ and, considering all mainshocks, we construct its distribution (Fig.3a). Interestingly we find that the support of the distribution of ΔF substantially presents only positive values, indicating that for all mainshocks we almost never find a region with $F_{k'}^{\rm pre}(t_k) > F_k^{\rm pre}(t_k)$. We can therefore conclude that, in the large majority of cases, the slipped area is the region with the highest pre-stress level on the fault, supporting the idea that the largest hazard must be associated to the most stressed region. However the actual level of the stress on a fault is practically inaccessible in real world experiments. At the same time, assuming a roughly constant tectonic loading, the stress level is expected to be roughly proportional to the time distance since the last earthquake, an information which is much more easy to achieve experimentally. Accordingly, we also introduce the quantity

$$T_k^{\rm pre}(t) = \sum_{i \in C(R, x(k))} \left(t - t_k^{last}(i)\right) \tag{4}$$

where $t_k^{last}(i)$ is the last time, before t_k, that the site i has been involved in a slipping process. We adopt the same definition of $C(R, x(k))$ as above and therefore $T_k^{\rm pre}$ is a measure of the average temporal distance from the last slip of the region internal to the circle $C(R, x(k))$. As in the analysis of Fig.3a we also compute the quantity $T_{k'}^{\rm pre}$ centering the circle in a random position x_{ran} and we plot the distribution of $T_k^{\rm pre} - T_{k'}^{\rm pre}$ in Fig.3b. We recover a pattern very similar to Fig.3a, with the support of the distribution

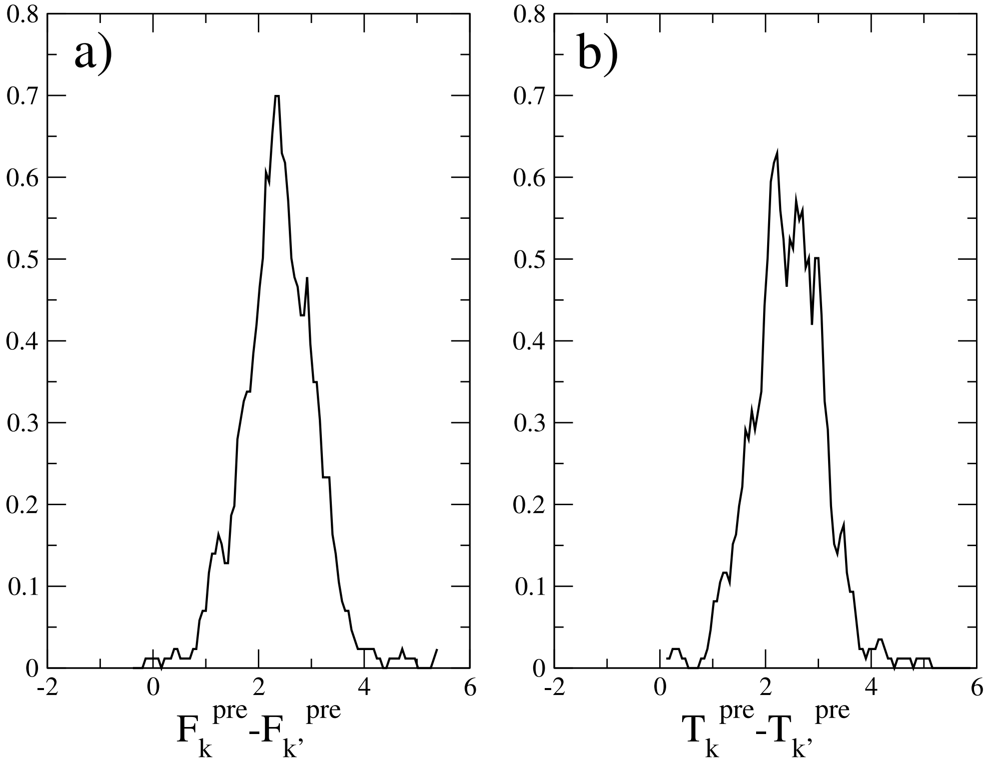

Figure 3. The distribution of $F_k^{\rm pre} - F_{k'}^{\rm pre}$ (panel (a)) and the distribution of of $T_k^{\rm pre} - T_{k'}^{\rm pre}$ (panel (b)). Both distributions are obtained considering 1000 mainshocks and 1000 different random positions x_{ran} for each mainshock.

presenting only positive values. Unexpectedly, the distribution of $T_k^{\rm pre}(t_k) - T_{k'}^{\rm pre}(t_k)$ is even more shifted towards the right than the distribution of $F_k^{\rm pre}(t_k) - F_{k'}^{\rm pre}(t_k)$. Results of Fig.3 clearly show that the region hosting the future mainshock is with a very high probability a gap region, i.e. the region with the largest value of $T_k^{\rm pre}$. We remark that in our model the shear stress rate is homogeneous in space and constant in time and that, for a more appropriate definition of the average temporal distance since the last slip, $T_k^{\rm pre}(t_k)$ must be multiplied by the average value of the shear stress rate, where averaging must be performed both in space, over the circle $C(R, x(k))$, and in time. Accordingly, in real word seismicity, the comparison between different patches of the same fault and/or of different faults is much more complicated than in our model.

3.2 Time evolution to the next instability

Fig.3 shows that at the time of instability, the region which hosts the impending earthquake is very frequently a gap region. However it also shows the existence of regions with similar stress conditions ($F_{k'}^{\rm pre} \simeq F_k^{\rm pre}$) or similar time delay since the last shock ($T_{k'}^{\rm pre} \simeq T_k^{\rm pre}$) that will experience a mainshock only at much later times. This implies that the hypothesis of alternation only holds probabilistically. This feature is clearly enlightened by the temporal evolution of the stress as the mainshock is approaching. At variance with the previous section when the time was fixed at the onset of the next mainshock change in space, now we consider a fixed space region, i.e. the circle $C(R, x(k))$, and study the evolution of $F_k^{\rm pre}$ and $F_k^{\rm pre}$ at different times. In particular, we consider the quantity $F_k^{\rm pre}(t)$, defined in Eq.3, at different time distances $t = t_k - \delta t$ from the k-th mainshock. It represents the stress level in the region that will host the subsequent mainshock, evaluate a time δt before the mainshock occurrence. We have then evaluated $F_k^{\mathrm{pre}}(t_k - \delta t)$ for all the 1000 mainshocks and obtained its probability density, defined as the number of mainshocks with $F_k^{\mathrm{pre}}(t_k - \delta t)$ in a given interval $[F, F + \delta F)$ divided by 1000 and by δF. We plot results in Fig.4a for δt values ranging from $\delta t = 15$, corresponding to the typical waiting time between two mainshocks, to $\delta t = 0$, i.e. at the onset of the mainshock occurrence. We observe that the distribution presents a Gaussian shape which is substantially independent of δt with a roughly constant standard deviation and a mean value which monotonically increases as δt approaches zero. In particular we find that values of $F_k^{\mathrm{pre}}(t) \gtrsim 4.4$ are observed only when $\delta t = 0$, signalling the imminence of a mainshock in that area. Nevertheless, several mainshocks are also observed to occur when $F_k^{\mathrm{pre}}(t) \lesssim 4.2$, when in the majority of cases the mainshock is observed at a much later times. This clearly shows that the hypothesis of alternation holds on average since there is a non-null probability to observe a mainshock in a region with a relatively small stress level. This feature becomes even more pronounced when we consider the evolution of the distribution of $T_k^{\mathrm{pre}}(t_k - \delta t)$ at different δt. In this case, indeed, the distribution is broad at all times δt and in particular we find a clear intersection between the distributions evaluated at $\delta t = 15$ and the one at $\delta t = 0$. This implies that it is probable to have a mainshocks such as its hosting region already presents at a time $\delta t = 15$, i.e. much before the occurrence of the mainshock, a gap value $T_k^{\mathrm{pre}}(t)$ which is larger than the one observed, for other mainshocks, immediately before their occurrence ($\delta t = 0$). We therefore find that the time distance to the next failure, i.e. δt, of a given region $C(R, x(k))$, is only weakly correlated to the time distance from the previous failure, i.e. $T_k^{\mathrm{pre}}(t)$. This result does not contradict the one of Fig.3: at a given time a mainshock has an higher probability to occur in a gap region but the temporal organization of mainshocks is not trivial and the value $T_k^{\mathrm{pre}}(t)$ does not univocally determine how close the region is to failure. Indeed Fig.4b shows that the probability that, conditioned to the local value of $T_{mes} = T_k^{\mathrm{pre}}$ measured at a given time t, the next big mainshock will occur in that region at the subsequent time $t + \delta t$, is very low. This probability can be however obtained from the intersection point of the vertical line passing for $T_{mes} = T_k^{\mathrm{pre}}$ with the curves at different δt in Fig.4b.

Summarizing, we find that even if in our model tectonic loading is constant, the occurrence of mainshocks is not periodic in time but is broad distributed. This feature can be also enlightened by considering the distribution of recurrence times between overlapping mainshocks. More precisely we define that two $m > m_{th}$ mainshocks j and k overlap if the distance between their epicenters is smaller than the maximum between R_j and R_k. In other words, one epicenter must be located within the slipping area of the other mainshock. We then define $\Delta t_{j,k}$ as the temporal distance between a mainshock k and its subsequent overlapping mainshock j. The probability density function of $\Delta t_{j,k}$ is plotted in Fig.5 as function of the normalized recurrence time, obtained by dividing $\Delta t_{j,k}$ by its average value $\langle \Delta t_{j,k} \rangle$. If we set $m_{th} = 3.5$, which is sufficiently large to have $A_k(\chi = 0) > A^{th} = L_y^2$, we find (Fig.5a) that the probability density distribution presents a peak around $\Delta t_{j,k} \simeq \langle \Delta t_{j,k} \rangle$, indicating a quasi-periodic behavior. The probability density distribution is however broad presenting, with non-vanishing frequency, recurrence times as smaller as $0.1 \langle \Delta t_{j,k} \rangle$ and also as large as $3 \langle \Delta t_{j,k} \rangle$. Interestingly the behavior of the probability density distribution of the numerical catalog appears in qualitative agreement with the one obtained by (Roth et al., 2017) from the historical record of $m > 8$ earthquakes along the South American subduction zone. A more quantitative comparison between the numerical and the historical distribution is meaningless since, as anticipated in the introduction, the historical distribution is obtained with only 20 recurrence times. At the same time, by considering a smaller $m_{th} = 3$ we find (Fig.5b) the presence of a peak at $\Delta t_{j,k} \simeq 0$ indicating short-time clustering reminiscent of the one obtained from historical data of (Roth et al., 2017) when all $m > 7$ earthquakes are included in the analysis. In our data set the peak at short time is caused by $m > 3$ aftershocks which occur close in space to the mainshock, causing their spatial overlap with it, and also close in time, leading to $\Delta t_{j,k} \simeq 0$.

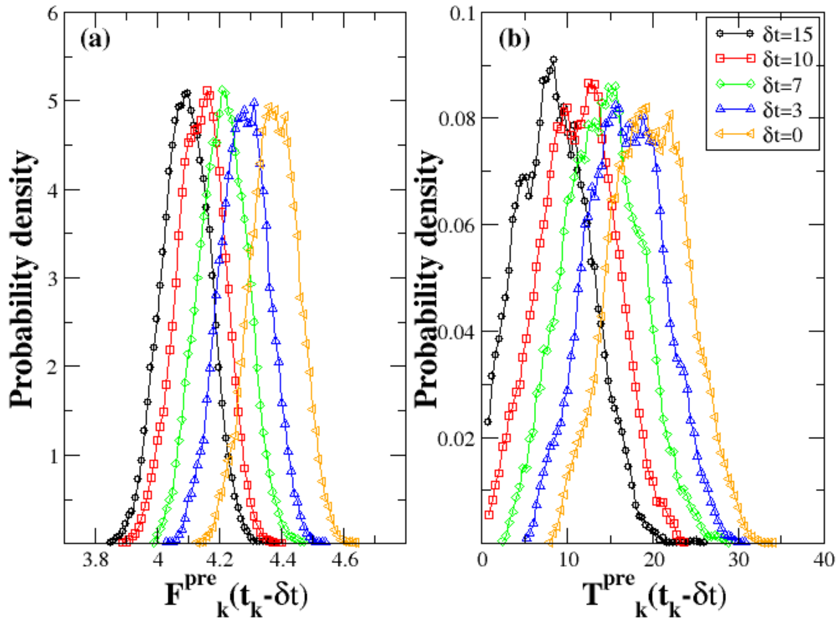

369 **Figure 4.** (a) The probability density of the stress level $F_k^{\mathrm{pre}}(t_k - \delta t)$ inside a region of size
370 R_k centered in the mainshock epicenter evaluated at a time distance δt before the mainshock
371 occurrence. (b) The probability density of the average time delay $T_k^{\mathrm{pre}}(t_k - \delta t)$ inside a region of
372 size R_k centered in the mainshock epicenter evaluated at a time distance δt before the mainshock
373 occurrence. Different curves correspond to different δt values (see the legend).

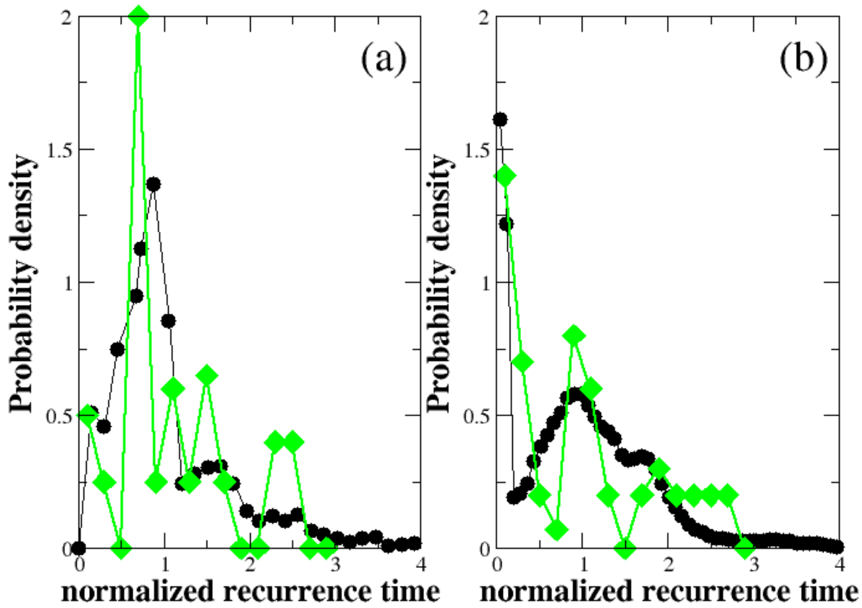

Figure 5. The probability density of recurrence times between successive overlapping earthquakes is plotted as function of recurrence times divided by their average. Black circles are used for data from the numerical catalog considering earthquakes with magnitude $m \geq 3.5$ which are sufficiently large to break all the seismogenic depth ($A_k(\chi = 0) \gtrsim L_y^2$) in panel (a) and considering all $m \geq 3$ earthquakes in panel (b). Filled green diamonds represent the same quantity extrapolated from Fig.4 of (Roth et al., 2017) obtained from historical data of the South American subduction zone considering $m \geq 8$ earthquakes in panel (a) and $m \geq 7$ earthquakes in panel (b).

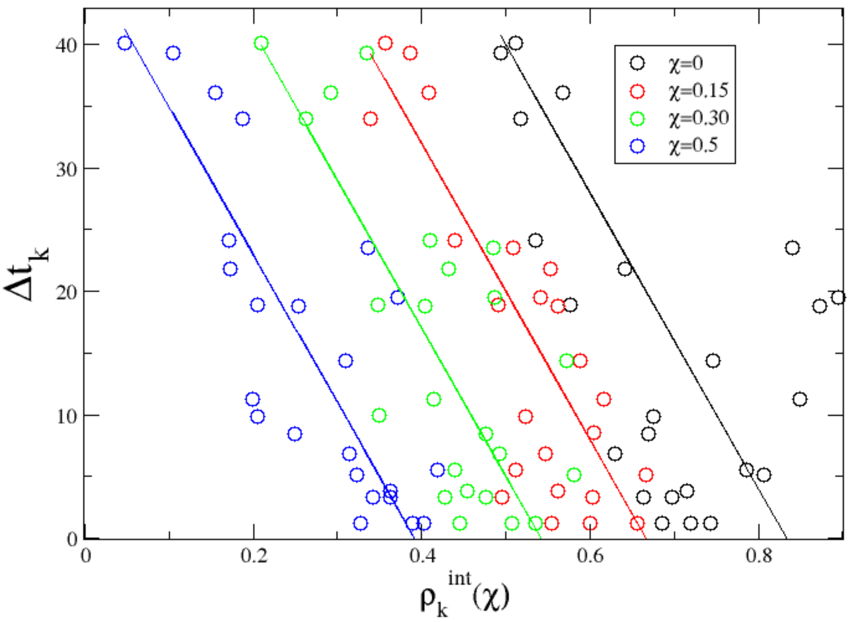

Figure 6. The parametric plot of Δt_k versus $\rho_k^{int}(\chi)$. Different colors correspond to different values of χ. Colored continuous lines represents the best linear fit $\Delta t_k = T_M - 120\rho_k^{int}(\chi)$, for each data set with $T_M = 101, 79, 65, 47$ for $\chi = 0, 0.15, 0.3, 0.5$, respectively.

3.3 The temporal distance until the next mainshock

We next explore the conjecture (Wetzler et al., 2018) that an excess of interior aftershocks could indicate a smaller stress drop of the mainshock and therefore a shorter time for the reactivation of the fault patch. For this kind of analysis we first evaluate the percentage of interior aftershocks of the k-th mainshock, $\rho_k^{int}(\chi)$, defined as the ratio between aftershocks with $\Delta r_{j(k),k}(\chi) < 0$ and the total aftershock number n_k^{aft}. We then assume that a subsequent mainshock j slips over the region involved by the slip process of a previous mainshock k, if $Q_{k,j}(\chi = 0) > 0.5A_j(\chi = 0)$. This criterion corresponds to the condition that two mainshocks are overlapping if there exists an overlap larger than the 50% between their slipping regions. We next indicate with $\Delta t_k = t_j - t_k$ the waiting time between two subsequent overlapping mainshocks and in Fig.6 we present the parametric plot of Δt_k versus $\rho_k^{int}(\chi)$, for all overlapping mainshocks in the numerical catalog. Results clearly enlighten the correlation between Δt_k and $\rho_k^{int}(\chi)$ supporting the prediction that a larger percentage of interior earthquakes (larger $\rho_k^{int}(\chi)$) indicates a smaller waiting time Δt_k to the next repeated mainshock. This result holds for all considered values of χ and for instance, for $\chi = 0.5$, we find that the waiting time to the next mainshock is of order of $100t_d$ when the percentage of interior aftershocks are larger than the 40% and becomes about 400 times larger ($4E5t_d$) when this percentage is smaller than the 10%. Even if data are scattered, a linear fit $\Delta t_k = T_M - \phi_M \rho_k^{int}(\chi)$ appears consistent with data, with $\phi_M \simeq 120$ independent of χ and $T_M \in [47, 101]$ according to the χ value. This information can be very useful to improve mainshock forecasting.

4 Discussion and Conclusions

Large earthquakes are rare events and this prevents the development of efficient forecasting models based only on the statistical information provided by the few historical large earthquakes. Therefore, the only possibility to make a skilful forecasting, without waiting to collect data for decades or even centuries, is to recast to physical models. The identification of the correct model is therefore a fundamental step preliminary to the formulation of a good forecasting hypothesis. In particular, the gap model originates from the description of the fault as a single block driven at a constant rate under a constant Coulomb friction. Within this description, indeed, the block will perform slips of equal size at regular time intervals. The model however neglects several key features of earthquake triggering such as time-dependent stress transfer mechanisms, which are responsible for aftershock occurrence, as well as heterogeneity in friction level and in the stress drop, etc... Roth et al. has already shown that the description of the fault as a single block under a rate-and-state friction law, after implementing an heterogeneous instead of constant stress drop, leads to a temporal organization of large events in much better agreement with experimental recurrence times. In their study, however, the length of the slipping patch is not controlled by the pre-existing stress condition but it is imposed by hand to be consistent with the GR law. The GR law, conversely, spontaneously originates within the BK description of the fault where many blocks are assumed to be elastically connected within each other (de Arcangelis et al., 2016). Starting from this description and taking into account friction heterogeneity together with the coupling with a more ductile layer where afterslip occurs, here we present a a model that also reproduces realistic feature of aftershock occurrence in space, time and magnitude. The model appears the appropriate numerical laboratory where forecasting hypotheses can be tested and validated. In this study, in particular, we have tested the hypothesis of alternation formulated by Gilbert (1909) more than 120 years ago and stating that "the next great seismic event in the same seismic district was more likely to occur at some other place". Our model shows that even if we implement a shear stress rate which is uniform in space and constant in time, the *characteristic* scenario where large earthquakes are roughly periodic in time must be discarded. Nonetheless, even if the time distance to the next failure is weakly correlated to the time distance from the previous earthquake, we find that the next large earthquake has an higher probability to be hosted by a gap region. Furthermore our study demonstrates the usefulness of aftershocks to have insights on the timing of the next large earthquake, coherently with the direction identified by Wetzler et al. (2018) from real world seismic data. In particular, our results provide further support to the scenario presented in Fig.8B of Wetzler et al. (2018) corresponding to a deficiency of aftershock activity within the core of the coseismic slip area, and a concentration near the perimeter. As concluding by Wetzler et al. (2018), even if this interpretation provides the best description of real world seismicity, other scenarios could not be completely excluded because of the uncertainty in slip areas and aftershock locations. In our numerical study these problems are not present and the deficiency of aftershocks is clearly proven. Moreover we also demonstrate the validity of the conjecture proposed by Wetzler et al. (2018) that the temporal distance to the subsequent large earthquake is smaller the larger is the percentage of aftershocks inside the high slip contour of the mainshock.

More generally the preented model can be used to validate patterns that, because of instrumental uncertainties, emerge less clearly from real world data. For instance, the model exhibits (Petrillo et al., 2020) a decrease in the b-value of the GR law during pre-mainshock seismicity which has been also proposed as a distinct feature of instrumental foreshocks (Gulia & Wiemer, 2019; Lippiello, Petrillo, & Godano, 2021). A better understanding of these patterns in the physical model can be fundamental to better test this hypothesis in instrumental data.

At the same time the agreement between spatial patterns of numerical and instrumental aftershocks suggests that the mechanism responsible for aftershock triggering is correctly implemented in our model. This represents a further support to the hypothesis that aftershocks are induced by afterslip (Perfettini & Avouac, 2004, 2007; Lippiello et al., 2019; Petrillo et al., 2020; Lippiello, Petrillo, Landes, & Rosso, 2021). On the other hand, the model we present neglects many features of real fault systems. As an example, it considers an isolated fault ignoring the interaction among different faults which can cause a time advance or delay to the next mainshock and it assumes a constant and homogeneous shear stress rate. This makes the application of our findings to real world seismic occurrence not straightforward.

Acknowledgments

This research activity has been supported by the Program VAnviteLli pEr la RicErca: VALERE 2019, financed by the University of Campania “L. Vanvitelli”. E.L. and G.P. also acknowledge support from MIUR-PRIN project ”Coarse-grained description for non-equilibrium systems and transport phenomena (CO-NEST)” n.201798CZL.

Author contributions: E.L., G.P. and A.R. have all contributed extensively to numerical simulations, data analysis and to write the manuscript.

Data availability: The source code of the numerical model is available from the corresponding author. Numerical data that support the findings of this study are available from the corresponding author upon reasonable request.

References

Burrige, R., & Knopoff, L. (1967). Model and theoretical seismicity. *Bullettin of the Seismological Society of America*(57), 341–371.

Chris, M. (1998). Laboratory-derived friction laws and their application to seismic faulting. *Annual Review of Earth and Planetary Sciences*, *26*, 643-696. doi: 10.1146/annurev.earth.26.1.643

de Arcangelis, L., Godano, C., Grasso, J. R., & Lippiello, E. (2016). Statistical physics approach to earthquake occurrence and forecasting. *Physics Reports*, *628*, 1 - 91. Retrieved from `//www.sciencedirect.com/science/article/pii/S0370157316300011` doi: http://dx.doi.org/10.1016/j.physrep.2016.03.002

Dieterich, J. H. (1972). Time-dependent friction as a possible mechanism for aftershocks. *Journal of Geophysical Research*, *77*(20), 3771–3781. Retrieved from `http://dx.doi.org/10.1029/JB077i020p03771` doi: 10.1029/JB077i020p03771

Gilbert, G. K. (1909). Earthquake forecasts. *Science*, *29*(734), 121–138. Retrieved from `http://www.jstor.org/stable/1635153`

Gulia, L., & Wiemer, S. (2019). Real-time discrimination of earthquake foreshocks and aftershocks. *Nature*, *574*, 193-199. doi: 10.1038/s41586-019-1606-4

Jagla, E. A. (2010, Apr). Realistic spatial and temporal earthquake distributions in a modified Olami-Feder-Christensen model. *Phys. Rev. E*, *81*, 046117. Retrieved from `http://link.aps.org/doi/10.1103/PhysRevE.81.046117` doi: 10.1103/PhysRevE.81.046117

Jagla, E. A. (2011). Delayed dynamic triggering of earthquakes: Evidence from a statistical model of seismicity. *EPL (Europhysics Letters)*, *93*(1), 19001. Retrieved from `http://stacks.iop.org/0295-5075/93/i=1/a=19001`

Jagla, E. A. (2013, Dec). Forest-fire analogy to explain the b value of the Gutenberg-Richter law for earthquakes. *Phys. Rev. Lett.*, *111*, 238501. Retrieved from `http://link.aps.org/doi/10.1103/PhysRevLett.111.238501` doi: 10.1103/PhysRevLett.111.238501

Jagla, E. A. (2014, Oct). Aftershock production rate of driven viscoelastic interfaces. *Phys. Rev. E*, *90*, 042129. Retrieved from `http://link.aps.org/doi/10.1103/PhysRevE.90.042129` doi: 10.1103/PhysRevE.90.042129

Jagla, E. A., & Kolton, A. B. (2010). A mechanism for spatial and temporal earthquake clustering. *Journal of Geophysical Research: Solid Earth*, *115*(B5), B05312. Retrieved from `http://dx.doi.org/10.1029/2009JB006974` doi: 10.1029/2009JB006974

Kagan, Y. Y., & Jackson, D. D. (1991). Seismic gap hypothesis: Ten years after. *Journal of Geophysical Research: Solid Earth*, *96*(B13), 21419-21431. Retrieved from `https://agupubs.onlinelibrary.wiley.com/doi/abs/10.1029/91JB02210` doi: https://doi.org/10.1029/91JB02210

Landes, F. m. c. P., Rosso, A., & Jagla, E. A. (2015, Jul). Frictional dynamics of viscoelastic solids driven on a rough surface. *Phys. Rev. E*, *92*, 012407. Retrieved from `http://link.aps.org/doi/10.1103/PhysRevE.92.012407` doi: 10.1103/PhysRevE.92.012407

Landes, F. P. (2016). Viscoelastic interfaces driven in dosordered media. *Springer Theses*. doi: 10.1007/978-3-319-20022-4

Landes, F. P., & Lippiello, E. (2016, May). Scaling laws in earthquake occurrence: Disorder, viscosity, and finite size effects in olami-feder-christensen models. *Phys. Rev. E*, *93*, 051001. Retrieved from `https://link.aps.org/doi/10.1103/PhysRevE.93.051001` doi: 10.1103/PhysRevE.93.051001

Lippiello, E., Giacco, F., Marzocchi, W., Godano, C., & de Arcangelis, L. (2015). Mechanical origin of aftershocks. *Scientific Reports*, *5*, 1-6.

Lippiello, E., Petrillo, G., & Godano, C. (2021). Recognizing the waveform of a mainshock. *Nature Geoscience*.

Lippiello, E., Petrillo, G., Landes, F., & Rosso, A. (2019). Fault heterogeneity and the connection between aftershocks and afterslip. *Bulletin of the Seismological Society of America*, *109*(3), 1156–1163.

Lippiello, E., Petrillo, G., Landes, F., & Rosso, A. (2021). The genesis of aftershocks in spring slider models. , 131-151. Retrieved from `https://onlinelibrary.wiley.com/doi/abs/10.1002/9781119825050.ch5` doi: https://doi.org/10.1002/9781119825050.ch5

McCann, W., Nishenko, S., Sykes, L., & et al. (1979). Seismic gaps and plate tectonics: Seismic potential for major boundaries. *PAGEOPH*, *117*, 1082–1147. doi: 10.1007/BF00876211

Mulargia, F., Stark, P. B., & Geller, R. J. (2017). Why is probabilistic seismic hazard analysis (psha) still used? *Physics of the Earth and Planetary Interiors*, *264*, 63-75. Retrieved from `https://www.sciencedirect.com/science/article/pii/S0031920116303016` doi: https://doi.org/10.1016/j.pepi.2016.12.002

Nishenko, S. (1991). Circum-pacific seismic potential: 1989–1999. *PAGEOPH*, *135*, 169–259. doi: 10.1007/BF008802409

Olami, Z., Feder, H. J. S., & Christensen, K. (1992, Feb). Self-organized criticality in a continuous, nonconservative cellular automaton modeling earthquakes. *Phys. Rev. Lett.*, *68*, 1244–1247. Retrieved from `http://link.aps.org/doi/10.1103/PhysRevLett.68.1244` doi: 10.1103/PhysRevLett.68.1244

Omori, F. (1894). On the after-shocks of earthquakes. *J. Coll. Sci. Imp. Univ. Tokyo*, *7*, 111-200.

Perfettini, H., & Avouac, J. (2007). Modeling afterslip and aftershocks following the 1992 Landers earthquake. *Journal of Geophysical Research: Solid Earth*, *112*(B7). Retrieved from `https://agupubs.onlinelibrary.wiley.com/doi/abs/10.1029/2006JB004399` doi: 10.1029/2006JB004399

Perfettini, H., & Avouac, J.-P. (2004). Postseismic relaxation driven by brittle creep: A possible mechanism to reconcile geodetic measurements and the decay rate of aftershocks, application to the Chi-Chi earthquake, Taiwan. *Journal of Geophysical Research: Solid Earth*, *109*(B2), B02304. Retrieved from http://dx.doi.org/10.1029/2003JB002488 doi: 10.1029/2003JB002488

Petrillo, G., Landes, F., Lippiello, E., & Rosso, A. (2020). The influence of the brittle-ductile transition zone on aftershock and foreshock occurrence. *Nature Communications*, *11*, 3010. doi: 10.1038/s41467-020-16811-7

Rong, Y., Jackson, D. D., & Kagan, Y. Y. (2003). Seismic gaps and earthquakes. *Journal of Geophysical Research: Solid Earth*, *108*(B10). Retrieved from https://agupubs.onlinelibrary.wiley.com/doi/abs/10.1029/2002JB002334 doi: https://doi.org/10.1029/2002JB002334

Roth, F., Dahm, T., & Hainzl, S. (2017, 08). Testing stress shadowing effects at the South American subduction zone. *Geophysical Journal International*, *211*(2), 1272-1283. Retrieved from https://doi.org/10.1093/gji/ggx362 doi: 10.1093/gji/ggx362

Ruina, A. (1983). Slip instability and state variable friction laws. *Journal of Geophysical Research: Solid Earth*, *88*(B12), 10359–10370. Retrieved from http://dx.doi.org/10.1029/JB088iB12p10359 doi: 10.1029/JB088iB12p10359

van der Elst, N. J., & Shaw, B. E. (2015). Larger aftershocks happen farther away: Nonseparability of magnitude and spatial distributions of aftershocks. *Geophysical Research Letters*, *42*(14), 5771-5778. Retrieved from https://agupubs.onlinelibrary.wiley.com/doi/abs/10.1002/2015GL064734 doi: https://doi.org/10.1002/2015GL064734

Wetzler, N., Lay, T., Brodsky, E. E., & Kanamori, H. (2018). Systematic deficiency of aftershocks in areas of high coseismic slip for large subduction zone earthquakes. *Science Advances*, *4*(2). Retrieved from https://advances.sciencemag.org/content/4/2/eaao3225 doi: 10.1126/sciadv.aao3225

Zhang, X., & Shcherbakov, R. (2016). Power-law rheology controls aftershock triggering and decay. *Scientific Report*, *6*, 36668. doi: 10.1038/srep36668